

Effects of Spanwise Spacing on the Interaction of Tandem Pitching Hydrofoils

David S. Lee*

Lehigh University, Bethlehem, Pennsylvania 18015

John T. Hrynuk[†]

DEVCOM Army Research Laboratory, Aberdeen Proving Ground, Maryland 21005

Keith W. Moored, III[‡]

Lehigh University, Bethlehem, Pennsylvania 18015

https://doi.org/10.2514/1.J063077

The interaction between a pair of tandem in-line oscillating hydrofoils is presented. The hydrofoils undergo sinusoidal pitching about their leading edges with a fixed Strouhal number of St=0.25 and a Reynolds number of 10,000. The streamwise spacing, spanwise spacing, and phase offset between the hydrofoils are varied. Force measurements are employed to investigate changes in thrust, lift, spanwise force, power consumption, and propulsive efficiency. A method to mitigate confounding factors from connecting rod drag is employed using streamlined fairings. Near and far streamwise spacing regions are identified with a transition occurring near 0.875 chord lengths downstream. Decreasing streamwise spacing in the far region causes a rise in the maximum power consumption of the follower hydrofoil. Decreasing streamwise spacing in the near region results in an opposite trend, with a sharp drop in maximum average power consumption by the follower. An empirical model for power consumption of the follower is developed. Increased spanwise spacing is found to weaken the interaction between the hydrofoils, driving them toward their isolated performance. This phenomenon is related to the spanwise contraction of the wake shed by the leader and is a function of the overlap of the wake region impacting the follower.

Nomenclature

A = peak-to-peak trailing-edge amplitude of oscillation, m

AR = aspect ratio b = span length, m

 $C_{[*]}$ = dimensionless coefficient for quantity [*]

c = chord length, m

 F_z = force acting in the spanwise direction, N

f = frequency of oscillation, Hz k = reduced frequency; fc/U_{∞}

L = lift force, N

P = power consumption, W Re = Reynolds number; $U_{\infty}c/\nu$ St = Strouhal number; fA/U_{∞}

T = thrust force, N

 T_z = torque about axis of oscillation, N/m

 \tilde{U}_{∞} = freestream velocity, m/s

x/c = dimensionless streamwise spacing z/b = dimensionless spanwise spacing

 η = propulsive efficiency θ = pitch angle, deg

 θ_A = maximum pitch angle, deg $\dot{\theta}$ = angular velocity, deg/s

= angular velocity, deg/s = kinematic viscosity, 1 mm²/s

 ρ = density (1000 kg/m³) ϕ = phase offset, deg

Presented as Paper 2022-0330 at the AIAA SciTech 2022 Forum, San Diego, CA and Virtual, January 3–7, 2022; received 7 April 2023; revision received 22 June 2023; accepted for publication 7 August 2023; published online 5 September 2023. This material is declared a work of the U.S. Government and is not subject to copyright protection in the United States. All requests for copying and permission to reprint should be submitted to CCC at www.copyright.com; employ the eISSN 1533-385X to initiate your request. See also AIAA Rights and Permissions www.aiaa.org/randp.

*Graduate Student, Department of Mechanical Engineering and Mechanics; dsl316@lehigh.edu. Student Member AIAA (Corresponding Author).

[†]Research Mechanical Engineer, Combat Capabilities Development Command, Army Research Laboratory, Member AIAA.

*Associate Professor, Department of Mechanical Engineering and Mechanics; kmoored@lehigh.edu. Member AIAA.

I. Introduction

NY swimming or flying system will shed a wake as it passes A through a flow. When one system follows closely behind another, it will inherently interact with the wake shed by the leading system: an interaction which may drastically alter the performance of both systems. Steady aerodynamic interactions are commonly observed in the formation flight of fixed-wing aircraft where drag reduction is achievable [1]. Although commonly associated with military aircraft, these interactions have also been observed in nature. In one study, a group of pelicans were trained to glide in a "V"-shaped formation [2]. It was observed that the pelicans in formation achieved a farther glide distance as compared to what they could in isolation. Similarly, it has been observed that ibises flying in this optimal V-shaped formation will synchronize their wing beats to maximize beneficial upwash interactions, and thus conserve energy [3]. Another area where beneficial wake interactions are hypothesized to occur is fish schools. The specific nature of these interactions depends on the types of wakes produced and encountered within the school. Many fish swim with what is referred to as a carangiform profile, where the body remains largely static while the tail fin produces the majority of the thrust through pitching and heaving motions [4]. The type of wake produced by this form of propulsion is linked to the Strouhal number of $St = fA/U_{\infty}$, where f is the frequency of oscillation, A is the peak-to-peak amplitude of the oscillation, and U_{∞} is the incoming freestream velocity. In nature, fish have been observed to have tail oscillation frequencies and amplitudes corresponding to a relatively narrow band of Strouhal numbers: 0.2 < St <0.4 [5,6]. Experiments have shown that this range corresponds to a peak in propulsive efficiency and the presence of a reverse von Kármán vortex street. The transition from regular von Kármán wakes to reverse von Kármán wakes has been heavily studied [7-13], producing a wide range of wake names, with the wake generated by fish commonly referred to as a 2S (wake structures where two single vortices are produced each shedding cycle) wake [14]. Significant studies and numerous reviews have been done on the mechanisms of individual fish swimming [15–17], different simplified motions [14], and even on real fish in a controlled environment [18].

Fish are believed to school for a wide variety of reasons, including socialization, predator avoidance, and feeding [19–23]. The observation and study of fish schools have shown that fish have lower

tail-beat frequencies based on their positioning within a school suggests that they are deriving a hydrodynamic benefit and saving energy when schooling [24,25]. To date, however, direct measurements of the oxygen consumption (and therefore energy expenditure) of schooling fish remain an outstanding issue. Fish have also been observed to synchronize their tail beats relative to one another based on sensory feedback on the surrounding flow from their lateral line, which is a sensing organ somewhat unique to fish [26,27]. When fish are denied this sensory input, they have been observed to lose their tail-beat synchrony [28] and tend to remain further away from their neighbors while schooling [29]. Fish have also been observed to actively interact with other wakes in a flow, specifically adjusting their swimming gait downstream of cylinders [30]. Similar behavior has been observed in a fish following behind a purely pitching [31] or pitching and heaving hydrofoil producing fishlike wakes [32]. This behavior also emerges passively, which has been shown when a recently deceased fish was placed in the wake of a cylinder [18]. In this case, the flexible body of the fish, without internal or external control, interacted with the cylinder wake to produce net thrust. Recent works using adjoint optimization methods have also found that the drag on tandem oscillating cylinders in flow may be reduced by synchronizing their oscillations [33,34].

By leveraging engineering simplifications of fish swimming, an experimental study of infinite-span pitching hydrofoils in a constrained tandem configuration by Boschitsch et al. [35] demonstrated that the leading hydrofoil is largely unaffected by the presence of the follower, except in cases of streamwise spacings of less than one chord. In these close interaction cases, the leader experienced propulsive efficiencies up to 1.2 times what it experienced in isolation. The efficiency of the follower is always affected by both phase offset (between the oscillation motions) and streamwise spacing of the hydrofoils. In some cases, the combination of phase difference and spacing increased the efficiency of the following hydrofoil up to 1.5 times the isolated case. At each streamwise spacing, there was a specific phase offset that corresponded to a peak in efficiency for the follower. This phase was closely linked with the streamwise spacing of the hydrofoils, creating a banding effect in the streamwise spacing-phase offset space. Boschitsch et al. [35] also showed that the vortices shed by the upstream hydrofoil served to either enhance or reduce the thrust production of the follower. In time-averaged flow data, cases with high average thrust production resulted a single coherent jet oriented downstream. In cases with low average thrust production, a branched wake structure was present, where impinging vortices were pushed at an oblique angle to the hydrofoil, thus reducing net thrust.

Kurt and Moored [36] extended these studies by evaluating hydrofoil tip and finite-span model effects on performance of tandem hydrofoils. The flowfields, which were recorded along the midspan of the finite-span hydrofoil models, produced similar time-averaged wakes as the infinite-span studies [35]. Kurt and Moored [36] also analyzed the tandem hydrofoils for their collective performance gains, which assessed the total improvements or losses of the system. The finite-span hydrofoil models were significantly less efficient when compared with infinite-span hydrofoils, with the finite-span models having a collective efficiency of 25%, as compared to 42% for the infinite-span hydrofoils. This loss in efficiency may be due to the presence of the hydrofoil tip vortex system, which is known to alter the vortices present in infinite-span studies into a chain of vortices [12,37]. This effect also causes a contraction of these chains in the spanwise direction as these vortices convect downstream [37].

Recent studies on constrained and unconstrained propulsors have found evidence of the existence of stable equilibrium points for the relative positioning of free-swimming propulsors [38–45]. These studies have typically focused on constrained in-line swimmers [35,36] or free swimmers locked into a planar arrangement [39,45]. These equilibrium points represent positions that swimmers will naturally gravitate toward due to the influence of hydrodynamic forces, which can further result in changes to their hydrodynamic performance. In general, these studies have shown that in the streamwise and cross-stream directions, there are equilibrium points, which are a function of the relative phase and oscillating amplitude of the

propulsive bodies present in the flow. However, these studies have not accounted for changes in positioning outside the two-dimensional (2-D) oscillation plane in the spanwise direction.

The current study experimentally investigates the effects of spanwise spacing on tandem in-line thrust-producing hydrofoils. Similar to prior studies, oscillating hydrofoils were placed at fixed relative positions and tested with varied oscillation phase differences. The addition of spanwise spacing will show the effects of the vortex chain system generated by the leading propulsor and extend the search for equilibrium points in the spanwise direction. Force measurements at these relative positions are used to define "near" and "far" streamwise interaction regions, as well as document how spanwise shifts alter the performance of the hydrofoils.

II. Experimental Methods

Experiments were performed in a recirculating flow channel located at Lehigh University, which has a turbulence intensity of less than 0.3% of freestream velocity [46]. Finite-span hydrofoils were constructed out of polyethylene terephthalate glycol using a fused deposition modeling three-dimensional (3-D) printer and sanded to ensure a smooth surface finish. Both hydrofoils had a rectangular planform shape with a chord length of c = 9.5 cm and a span of b = 19 cm, resulting in an aspect ratio of AR = 2. The hydrofoils had a NACA 0012 profile with squared wingtips. Both hydrofoils were connected to servo motors using 10-mm-diameter carbon fiber rods. Their pitching axis was 5 mm behind the leading edge, or 5% of the chord. An acrylic plate was also fitted over the surface of the flow channel to mitigate free surface effects. The drag coefficient for these actuating rods was approximately $C_d \approx 0.095$ [47] and, with one chord of immersion in the flow, the drag they could produce was almost 50% of the expected thrust produced by the hydrofoils. In addition, the upstream, or leader, hydrofoil was manufactured with a longer actuating rod to facilitate changes in spanwise spacing between the hydrofoils. A key experimental feature was the addition of streamlined fairings placed around the actuating rods, which served to shield them from the oncoming flow, and thereby eliminate rod drag from the measured forces. This was more important in cases where the spanwise spacing was varied because the drag on differing rod lengths could result in inaccurate assessment of thrust production. Both fairings had teardrop profiles with overall lengths of 5.75 cm and a leading-edge diameter of 20 mm. The fairings were constructed in two parts. The first piece was affixed to the actuation mechanism mounting, whereas the second was attached to the first using magnets. The clearance between the actuation rods and the inner surface of the fairings was approximately 3 mm to ensure that the rods never came into contact with the fairings. Figures 1a–1b schematically show the actuation mechanisms used for both hydrofoils as well as the placement of the fairings. Figure 1c shows a photograph of the fitment of the rear portion of the fairing to one of the hydrofoils.

The hydrofoils were oscillated independently by high-torque servo motors (Dynamixel model MX-64AT), which have a minimum command-response resolution of 0.0879 deg. The oscillation motion was sinusoidal with an adjustable phase offset between the hydrofoils, which are given in Eqs. (1) and (2):

$$\theta_F = \theta_A \sin(2\pi f t) \tag{1}$$

$$\theta_L = \theta_A \sin(2\pi f t + \phi) \tag{2}$$

where θ_L and θ_F are the pitching angles at time t for the leader and follower, respectively; and θ_A is the angular amplitude of oscillation. Also, ϕ is the temporal phase offset between the leader's and follower's pitching motions. A phase offset of 0 deg indicates fully in-phase motion, and a phase offset of 180 deg indicates fully out-of-phase motion.

The experimental setup allowed for the streamwise spacing (x/c) and spanwise spacing (z/b) between the hydrofoils to be varied. Note that, here, the streamwise spacing is normalized by the chord length, whereas the spanwise spacing is normalized by the span

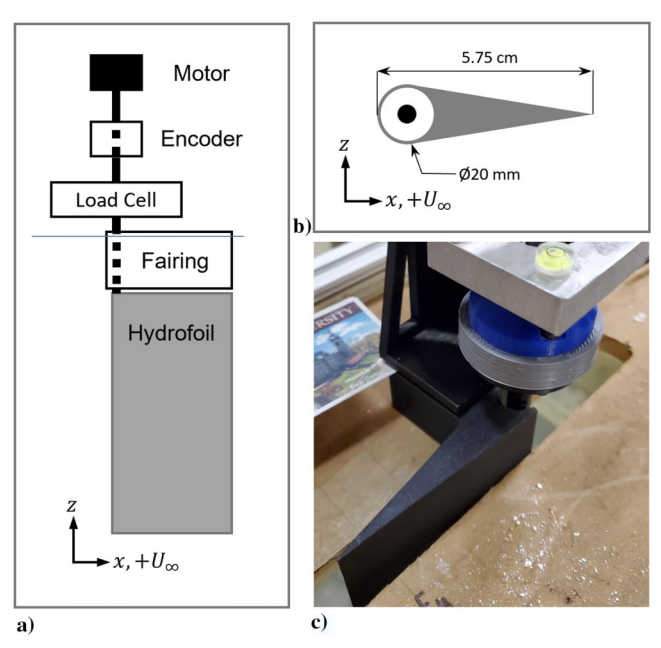
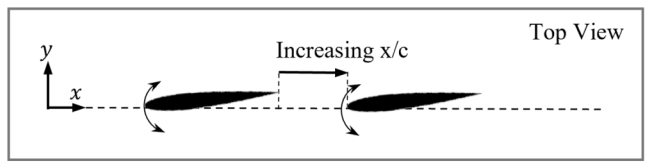


Fig. 1 Schematics of a) hydrofoil actuation linkages and b) schematic of fairing placement around actuation rod. Photograph of mounting of rear fairing portion (Fig. 1c).

length to facilitate discussion of the offset as percentages of the hydrofoil dimension in each direction. The spanwise spacings ranged from 0 to 0.5 spans in 0.125 increments. The streamwise spacing ranged from 0.625 to 1.125 chords in 0.125 increments. The hydrofoils were kept a minimum of one chord length from the channel floor and the surface plate. A schematic of the experimental setup can be seen in Fig. 2.

The hydrodynamic forces acting on the hydrofoils were measured using high-resolution six-axis load cells (ATI NANO43) fitted between the servo motors and hydrofoils. Using the manufacturer-supplied calibration matrices, the load cells were able to resolve forces as small as 1/512 N and torques as small as 1/40 N · mm. The sensor bias error supplied by the manufacturer was 1.25% for both load cells. The motions of the hydrofoils were recorded using quadrature optical encoders (USDigital E5 series) with a resolution of 5000 counts per revolution, or 0.0180 deg resolution using X4 decoding. The mean error between the command issued to the motors and the reading from the optical encoders was 0.05 deg. Data acquisition was conducted using a National Instruments PCI system at a sampling frequency of



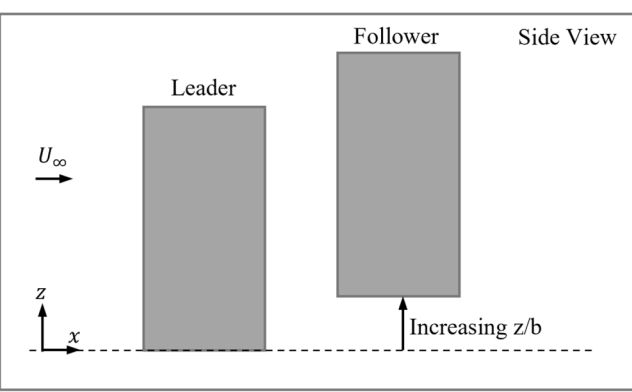


Fig. 2 Schematic of experimental setup.

Table 1 Experimental parameters

Parameter	Value
Foil profile	NACA 0012
c	9.5 cm
AR	2
$ heta_A$	$\pm 7.5 \deg$
f	1 Hz
U_{∞}	0.1 m/s
St	0.25
k	0.95
Re	10,000

1000 Hz. The load cells were tared in quiescent flow prior to each trial in this study. Instantaneous power consumption was calculated using

$$P(t) = T_Z \dot{\theta} \tag{3}$$

where P is the instantaneous power consumption, T_Z is the measured instantaneous torque about the oscillation axis, and $\dot{\theta}$ is the instantaneous angular velocity. The oscillating amplitude and frequency were kept fixed at $\theta_A=\pm7.5\,$ deg and $f=1\,$ Hz, respectively. The phase offset between the hydrofoils ranged from $\phi=0$ to 360 deg in 15 deg increments. Based on previous studies [35,36], the Strouhal number was held fixed at St=0.25, and the freestream velocity was set to $U_\infty=0.1\,$ m/s. These flow and motion conditions resulted in a Reynolds number of $Re=U_\infty c/\nu=10,000$, where ν is the kinematic viscosity, and a reduced frequency of $k=fc/U_\infty=0.95$. These values are summarized in Table 1.

Several common hydrodynamic forces are presented, including thrust T, lift L, and spanwise force F_Z . Forces were recorded in a reference frame relative to the load cells. A rotation matrix was then applied to give lift and thrust forces in the laboratory frame of reference:

$$T = -F_x \cos(\theta) + F_y \sin(\theta) \tag{4}$$

$$L = -F_{y}\cos(\theta) - F_{x}\sin(\theta) \tag{5}$$

where F_x and F_y are the x and y planar forces in the reference frame relative to the load cells. All forces were recorded in newtons and are presented in dimensionless form as

$$C_T = T/0.5\rho bc U_{\infty}^2 \tag{6}$$

$$C_L = L/0.5\rho bc U_{\infty}^2 \tag{7}$$

$$C_{F_Z} = F_Z / 0.5 \rho b c U_{\infty}^2$$
 (8)

where ρ is the fluid density. The power consumption was normalized as

$$C_P = P/0.5\rho bc U_{\infty}^3 \tag{9}$$

Time-averaged performance coefficients are denoted using overlines (for example, $\bar{[*]}$). The propulsive efficiency, presented as a percentage, was considered as the ratio of the average useful power output to the average power consumed as

$$\overline{\eta} = \overline{C_T}/\overline{C_P} \tag{10}$$

III. Results

A. Isolated Hydrofoil Performance

To verify the functionality of the experimental setup, data were taken for both hydrofoils in isolation, with only one hydrofoil in the flow at a time. The average thrust production $\overline{C_T}$, power consumption $\overline{C_P}$, and propulsive efficiency $\bar{\eta}$ were compared with those from previous studies and are shown in Table 2. Random uncertainties were based on standard deviations between 5 repeated trials: each with 40 repeated oscillation cycles. Bias and random uncertainties were determined using the methods outlined by Figliola and Beasley [48], and they are detailed in the Appendix. There were slight variations in the performance of the leader and follower hydrofoils, which were likely caused by minor variations in manufacturing of the hydrofoils, mounting hardware, and fairings. The leader hydrofoil was also fitted with a longer connecting rod to facilitate changes in spanwise spacing, which may also contribute to any difference. Prior experimental studies did not account for the offset drag of the static hydrofoil, and so values of C_T in Table 2 for the current study are adjusted using a drag offset of $C_D = 0.06$ for a NACA 0012 profile, which was derived from the work of Senturk and Smits [49]. The thrust aligned well with prior experiments by Kurt and Moored [36] but was somewhat lower than those predicted by Senturk and Smits [49], which was an infinite-span simulation. The power consumption measured in the current study matched well with those predicted by Senturk and Smits [49] but was noticeably lower than those reported by Kurt and Moored [36]. A number of factors likely reduced power consumption, including airfoil shape, Reynolds number, and the addition of fairings to the current study. Efficiency aligned reasonably well with prior studies while most closely aligning to the finitespan hydrofoils of Kurt and Moored [36].

B. Tandem Hydrofoils with Spanwise Spacing

The hydrofoils were placed in tandem in the flow channel and tested at a variety of streamwise and spanwise spacings. Figure 3 shows the relationship between the phase offset and the average performance coefficients of the leader and follower hydrofoils at x/c = 1.125chords of streamwise offset, which was the largest streamwise spacing tested in the current study. The variation in line color reflects the various spanwise spacings within the range of z/b = 0–0.5. Horizontal dashed lines identify the isolated hydrofoil mean performance coefficients. For the leader, the average thrust production and efficiency (Figs. 3a and 3c) were generally independent of phase offset. The average power consumption of the leader (Fig. 3b) had a minor dependence on the phase offset of the hydrofoils. Phase offsets of around $\phi = 180$ deg lowered power consumption slightly, whereas power consumption was increased above the isolated leader case for other phase offsets. Prior studies have shown that average performance coefficients of the follower are functions of phase offset [35,36], which is also the case for the follower here (Figs. 3d–3f). As in prior studies, the data exhibited a sinusoidal dependence on phase offset. The thrust and efficiency for both hydrofoils did not fall below their respective isolated values, but power consumption was observed to drop below the isolated values for some phase offsets.

The introduction of spanwise spacing had limited effects on the thrust and efficiency of the leader. However, the leader's power consumption consistently decreased with increasing spanwise spacing at all phase offsets. There were more noticeable effects on the follower when the spanwise spacing was varied. Three phase offsets of interest are noted by the vertical dashed lines in Fig. 3e: maximum average

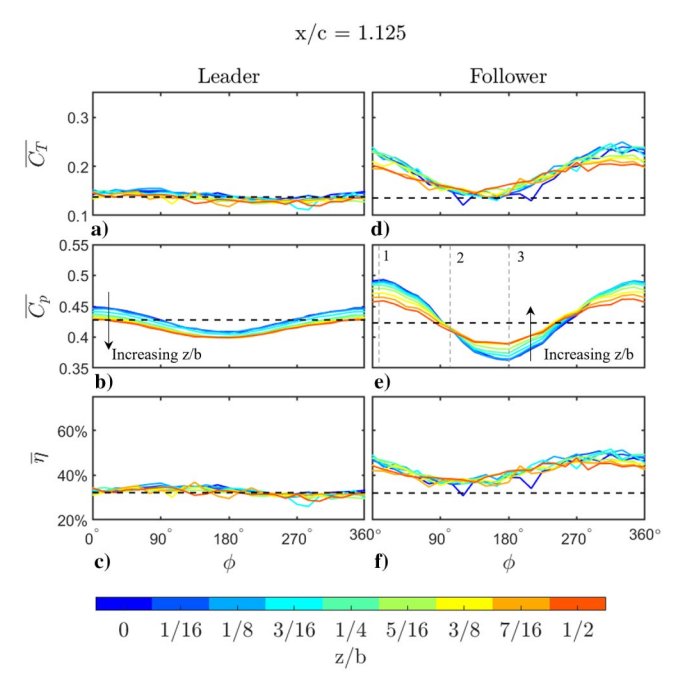


Fig. 3 Performance coefficients of tandem hydrofoils: x/c=1.125. Dashed lines denote performance in the isolated case.

power consumption near $\phi = 0$ deg (phase 1), average power consumption matching the isolated hydrofoil near $\phi = 90 \, \deg$ (phase 2), and minimum average power consumption near $\phi = 180 \, \deg$ (phase 3). The effects of spanwise spacing can be most easily observed at these three phase offsets, with the largest effect of spanwise spacing being observed in the power consumption. For the maximum average power consumption condition for the follower (phase 1), increasing the spanwise spacing reduced both the thrust production and power consumption of the follower. The corresponding decrease in efficiency indicates that the reduction in thrust production had an increased impact on the performance of the follower. Increasing the spanwise spacing at the minimum power condition (phase 3) caused an increase in power consumption with limited discernible changes in thrust production and efficiency. No changes were observed at the inflection phase offset (phase 2), but at this point, the hydrofoils acted nearly identically to two hydrofoils in isolation.

Similar trends were observed when the hydrofoils were moved closer together in the streamwise direction. Figure 4 shows the average performance coefficients for streamwise spacing of x/c=0.625, which was the closest tested. Both hydrofoils experienced greater variability in their average thrust production and efficiency, which is indicative of greater unsteadiness in the surrounding flow. The power consumption of the leader had a more pronounced sinusoidal dependence on phase offset than at larger streamwise spacing, with a substantial decrease in power consumption near $\phi=180$ deg. When increasing spanwise spacing, the amplitude of the leader's sinusoidal variation in power with phase offset was mildly reduced,

Table 2 Isolated performance metrics at $St = 0.25^a$

	Study	Reynolds number Re	Profile	$\overline{C_T}$	$\overline{C_p}$	$\overline{\eta}$
2-D experiment	Boschitsch et al. [35]	4,700	Teardrop	0.150 ± 0.020	0.660 ± 0.060	22 ± 4%
2-D experiment	Kurt and Moored [36]	4,800	Teardrop	0.140 ± 0.050	0.770 ± 0.001	$18\pm6\%$
2-D experiment	Kurt and Moored [36]	7,500	Teardrop	0.150 ± 0.020	0.790 ± 0.003	$19\pm2\%$
3-D experiment	Kurt and Moored [36]	7,500	Teardrop	0.210 ± 0.020	0.750 ± 0.005	$28\pm3\%$
2-D simulation	Senturk and Smits [49]	10,000	NACA 0012	0.161	0.429	38%
3-D experiment3-D experiment	Present study, leader Present study, follower	10,000 10,000	NACA 0012 NACA 0012	0.141 ± 0.016 0.136 ± 0.013	0.420 ± 0.040 0.423 ± 0.040	$33 \pm 3\%$ $32 \pm 1\%$

^aThe leader hydrofoil was at its maximum depth when tested in isolation.

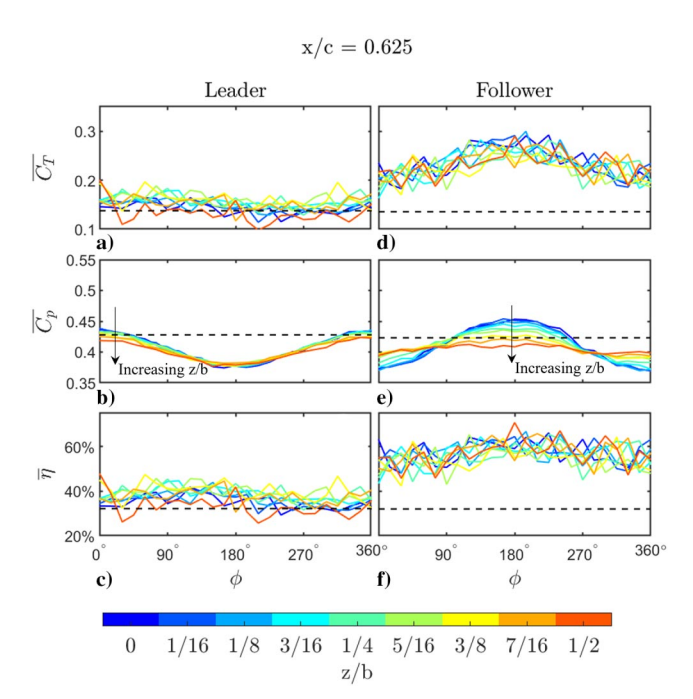


Fig. 4 Performance coefficients of tandem hydrofoils: x/c = 0.625. Dashed lines denote performance in the isolated case.

with the power decreasing around $\phi=0$ deg and increasing around $\phi=180$ deg. The thrust production and efficiency for the follower significantly increased for all phase offsets, with a peak in thrust occurring near $\phi=180$ deg. The phase offset of power consumption was shifted by approximately 180° , as compared with x/c=1.125 (Fig. 3), with the minimum and maximum power consumption occurring near $\phi=0$ and 180 deg, respectively. The effect of spanwise spacing on the follower power consumption was the same as that identified for x/c=1.125 in Fig. 3; that is, increasing spanwise spacing flattens the power consumption curve.

To better understand the parameter space, maximum average performance metrics are shown in Fig. 5 along with average magnitude

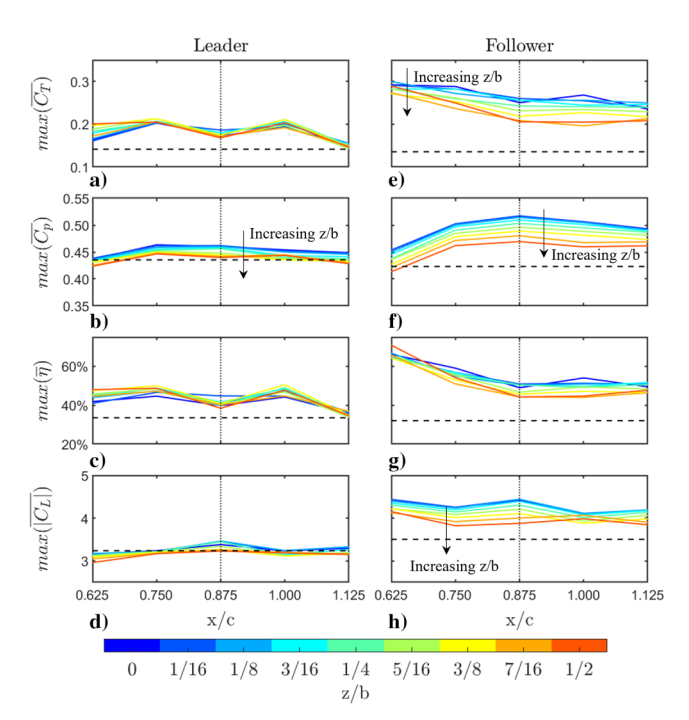


Fig. 5 Maximum performance coefficients and magnitude in lift of tandem hydrofoils. Dashed lines denote performance in the isolated case.

in lift coefficient $\overline{|C_L|}$ for each streamwise and spanwise combination. The lift values reported here represent the average magnitude of lateral forces experienced by the oscillating hydrofoils. The leader was largely insensitive to changes in streamwise and spanwise spacing but generally slightly outperformed the isolated hydrofoil case, regardless of follower position. All values for the follower (Figs. 5e-5h) were significantly higher than the isolated case. Regardless of streamwise position, increasing spanwise spacing caused performance metrics to shift toward the isolated case. Small changes in spanwise spacing around z/b = 0 caused seemingly no changes in values; but at larger z/b, changes in spacing generated notable decreases in all maximum values for the follower. Also of note is that in all arrangements tested, both the instantaneous and time-averaged spanwise forces $C_{F_{\pi}}$ for both hydrofoils were found to be small enough to be negligible, indicating no hydrodynamic forces pushing the hydrofoils toward any particular spanwise spacing in the time average.

Two distinct streamwise spacing regions are identified in Fig. 5, with the boundary occurring near x/c = 0.875 chords (vertical dotted lines). In the far region (x/c > 0.875 chords), the maximum thrust production and efficiency of the follower were independent of streamwise spacing. However, decreasing streamwise spacing in the far region corresponded to an increase in the maximum power consumption of the follower. In the near region (x/c < 0.875), the maximum thrust production, power consumption, and efficiency were functions of the streamwise spacing. The trend in maximum power consumption reversed from that in the far region, with decreasing streamwise spacing causing a sharp decrease in the follower's maximum power consumption. Decreasing streamwise spacing in the near region also corresponded to increases in the maximum achievable thrust production and efficiency for the follower. Lift appeared to be largely insensitive to changes in the streamwise spacing. Oscillating wings have been shown to be relatively insensitive to disturbances [50], suggesting that the vortex interaction here is not sufficiently large to alter lift-generating mechanisms.

C. Finite-Span Vortex Effect

The results shown so far reinforce those of previous studies, which found that the performance of tandem hydrofoils is heavily dependent on the streamwise spacing and phase offset relative to one another [35,36]. The results shown also demonstrate that the performances of the hydrofoils depend on their spanwise spacing relative to one another. This dependence is related to the structure of the wake shed by the leader. The wake structures shed by pitching hydrofoils have been well documented by prior studies, like the particle image velocimetry (PIV) results of King et al. [37]. Figure 6 shows a schematic of the wake structure expected to be shed by an isolated hydrofoil in this experiment. Hydrofoils undergoing periodic pitching motions at moderate Strouhal numbers are known to produce a nominally two-dimensional 2S wake structure at the midspan [37] with alternating sign vortices in the x-y plane, as shown in Fig. 6a. In addition, the wake shed from a finite-span oscillating hydrofoil experiences a spanwise contraction as it moves downstream. King et al. [37] observed that at St = 0.25, which is the same value as in the current experiments, the rate of the spanwise contraction of the wake was approximately 0.30 span lengths per chord length of the downstream movement. This prior result suggests that for a tandem interaction, such as the one in the current experiment, the amount of incoming wake directly impinging on the follower hydrofoil's span is directly proportional to the relative streamwise spacing between the hydrofoils, which accounts for the trends in x/c shown in Fig. 5.

The effect of spanwise spacing on the wake structure is shown in Fig. 7, which expands Fig. 6b. Figure 7 shows how the contraction of the incoming wake changes the amount of wake the follower interacts with. At streamwise spacings of x/c = 1 and z/b = 0, the wake shed by the leader interacts with 70% of the span of the follower, as shown in Fig. 7a. Small increases in spanwise spacing up to a critical z/b value of $z/b_{\rm crit} = 0.15$ do not change the percentage of the follower's span interacting with the incoming wake (Fig. 7c). However, increases in spanwise spacing beyond this value (Fig. 7b) decrease the portion of the follower's span interacting with the incoming wake.

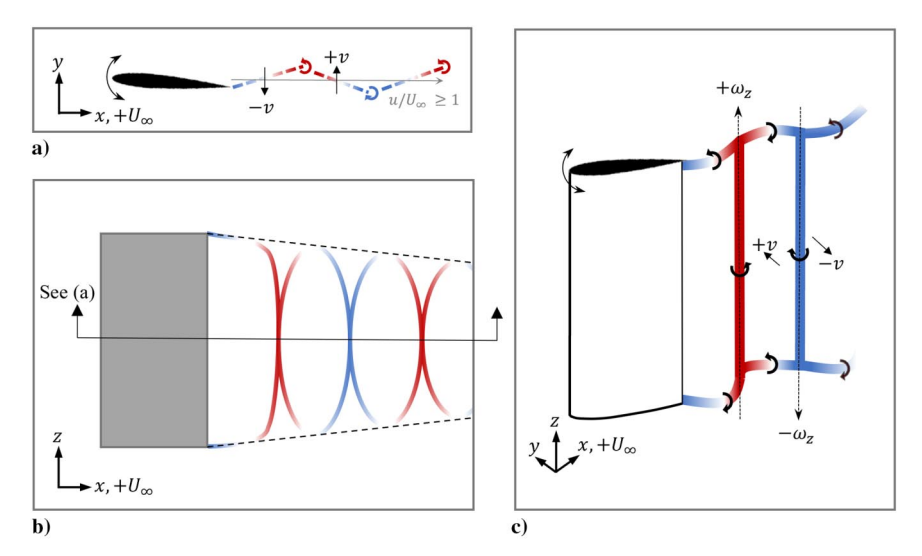


Fig. 6 Schematic representation of wake structure shed by isolated hydrofoil along a) midspan x-y plane and b) top-down x-z plane, as well as c) isometric view.

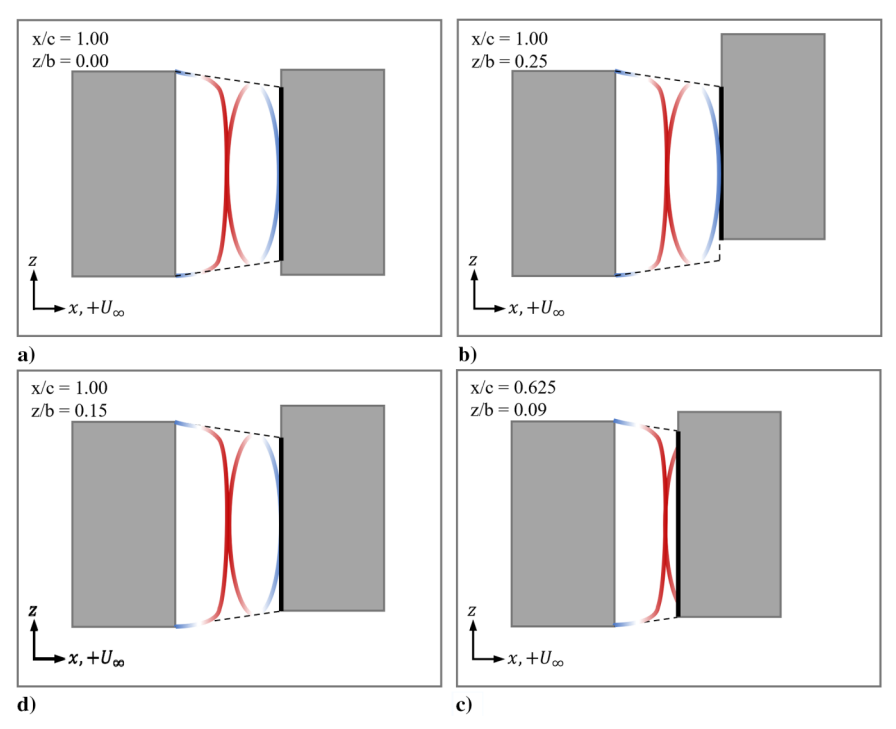


Fig. 7 X-Z plan view of portion of the leader's shed wake interacting with the follower hydrofoil.

This effect was observed in Fig. 5, where small changes in spanwise spacing around z/b=0 did not generate a significant change in the performance of the follower. Similarly, at x/c=0.625, the critical spanwise spacing was found to be $z/b_{\rm crit}=0.094$, as shown in Fig. 7d. This critical z/b value is a function of the wake contraction and can be defined by Eq. (11):

$$z/b_{\rm crit} = 0.15(x/c) \tag{11}$$

Figures 8b–8e show the maximum average performance of the follower hydrofoil at a streamwise spacing of x/c = 1.125, where $z/b_{\rm crit} = 0.169$ is denoted by the vertical dotted lines. At this streamwise spacing, the wake has contracted to approximately 66% of the follower's span. Figure 8a shows the fraction of the follower hydrofoil's span that is immersed in the wake of the leader hydrofoil. The dotted lines in Fig. 8 are included to draw attention to trends in the data. Small values of spanwise spacing $(0 \le z/b \le 0.169)$ resulted in

no change in maximum power consumption and lift magnitude, but slight increases in thrust production and efficiency were observed in Fig. 8b. This increase in performance is likely occurring when the tip vortex system from the leader aligns and suppresses the tip vortex of the follower hydrofoil, which would increase the follower's effective aspect ratio, thereby increasing its thrust production and efficiency. This region, where the performance of the follower was generally unchanged or slightly increased by changes in spanwise spacing, corresponds to cases where the amount of leader wake interacting with the follower remained constant. Conversely, increasing spanwise spacing above $z/b_{\rm crit}$ generated an approximately linear decrease in all performance coefficients.

Figure 9 recreates Fig. 8 for a closer streamwise spacing of x/c = 0.75. In this case, the thrust production (Fig. 9b) had more variability at all spanwise spacings. This is likely caused by the stronger vortex-body interaction taking place at the closer streamwise spacing. Figure 9 clearly shows how decreasing the streamwise spacing results in a smaller value of $z/b_{\rm crit}$, which aligns well with the

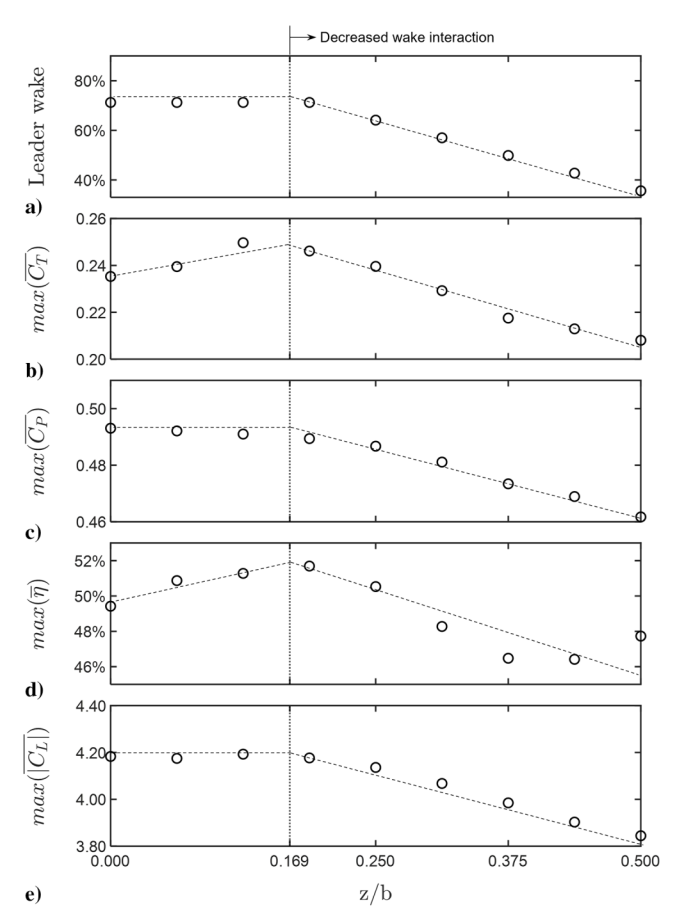


Fig. 8 Representations of a) amount of wake impinging on the follower hydrofoil, b) maximum average thrust production, c) power consumption, d) efficiency, and e) lift magnitude as functions of spanwise spacing at x/c=1.125. The dotted lines are included to draw attention to trends in the data.

prediction of Eq. (11) of $z/b_{\rm crit}=0.113$. Similar results were found for all other streamwise spacings considered. These results and those presented in Fig. 5 demonstrate a direct correlation between the strength of the tandem interaction on the follower hydrofoil and the portion of the follower hydrofoil's span interacting with the incoming wake.

D. Relationship Between Power, Phase, and Spanwise Spacing

A deeper analysis of the relationship between phase offset, streamwise spacing, and spanwise spacing was done to better understand the vortical interactions experienced by the follower. The average thrust production and power consumption of the follower hydrofoil at the minimum (z/b=0) and maximum (z/b=0.5) spanwise spacings are shown in Fig. 10. The boundary between the close and far regions was clearly visible in the data in this format and is noted by a dotted line at x/c=0.875. When considering the effects of spanwise spacing, both thrust production and power consumption had lower dependence on phase offset at large spanwise spacing (z/b=0.5) when compared to the in-line case (z/b=0). Despite this reduced dependence, the power consumption of the hydrofoils exhibited a linear relationship between phase offset and streamwise spacing that remained consistent across the various spanwise spacings tested (Figs. 10b and 10d).

The linear relationship in minimum power observed in Fig. 10 has been demonstrated to be a function of the vortex wake structure shed by the leader. Because the wake shed by the leader is periodic, a change in streamwise spacing was equivalent to a change in phase offset. Decreasing streamwise spacing, while holding the phase constant, will cause the vortex shed by the leader hydrofoil to impinge on the follower hydrofoil earlier in the follower's oscillation cycle, affecting the power consumption of the follower.

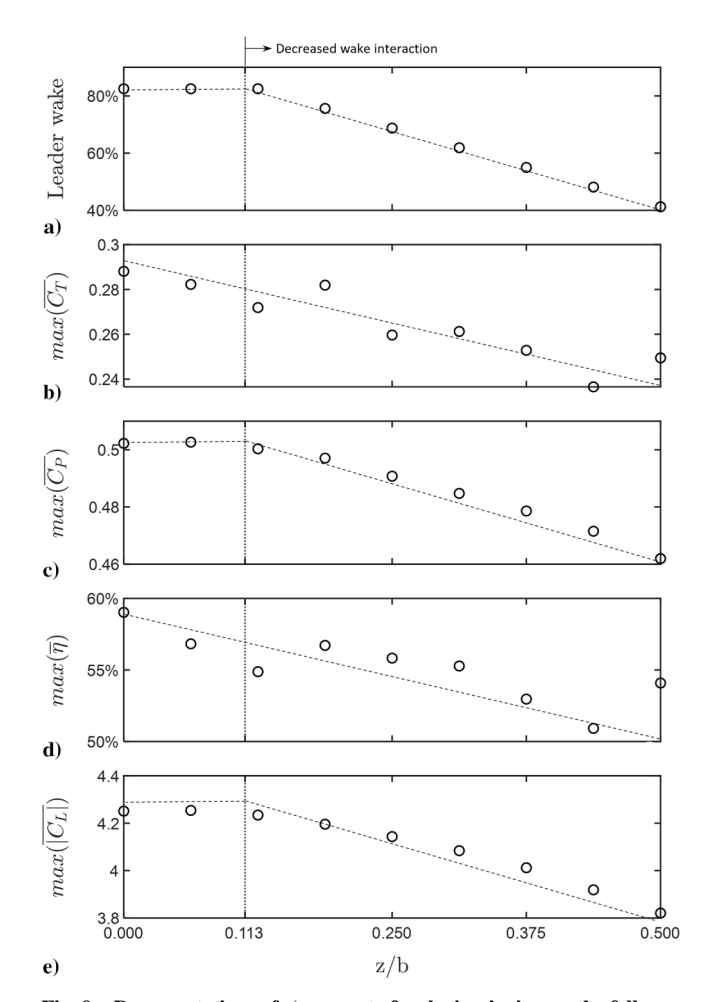


Fig. 9 Representations of a) amount of wake impinging on the follower hydrofoil, b) maximum average thrust production, c) power consumption, d) efficiency, and e) lift magnitude as functions of spanwise spacing at x/c=0.75. The dotted lines are included to draw attention to trends in the data.

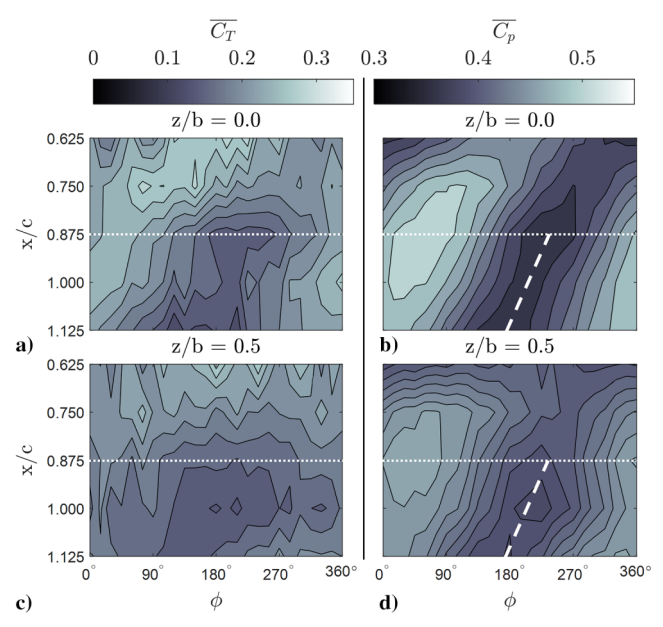


Fig. 10 Average thrust production and power consumption of follower hydrofoil.

Portugal et al. [3] expressed this concept as the simple linear relationship, which is given in Eq. (12):

$$\phi = -360 \operatorname{deg}(x/c)/\lambda^* + \phi_{\text{spatial}}$$
 (12)

where λ^* is the incoming wake wavelength normalized by the chord. The spatial phase ϕ_{spatial} is the equivalent phase offset, taking into account the number of wake wavelengths between the propulsors. This formulation was validated for tandem oscillating propulsors by Epps et al. [51]. Furthermore, this formulation was recently employed by Kurt and Moored [36] to determine the wake wavelength and the convective speed of the wake shed by a hydrofoil. Here, Eq. (12) was empirically applied to the phase offset at which minimum power consumption occurred in the far region data (shown in Figs. 10b and 10d as dashed lines) using a simple linear regression. The resulting phase for minimum power consumption for the tandem hydrofoils in this study is given in Eq. (13):

$$\phi_{\overline{C_R}, \min} = -240 \, \deg(x/c) + 435 \, \deg$$
 (13)

where $\phi_{\overline{C_P},\min}$ is the phase offset for minimum average power consumption for the follower as a function of x/c. Combining Eq. (13) with Eq. (12) to determine the wake wavelength, based on the power data, gives 360 deg $/\lambda^* = 240$ deg, and thus $\lambda^* =$ 1.4 chord lengths. The convective speed of the wake, based on this wake wavelength, was $1.4U_{\infty}$. Kurt and Moored [36] documented a wake convective speed of approximately $1.02U_{\infty}$ based on their PIV measurements of the wake of an isolated hydrofoil. A close analysis of the interaction PIV presented by Kurt and Moored [36] shows that in the far region, the wake wavelength increased when the vortices interacted with the follower. Figure 11 shows a schematic representation of this wake acceleration during the interaction. Interestingly, this phenomenon does not appear to be function of the phase offset between the hydrofoils. The phases at which the follower experienced minimum and maximum average power consumption (see Figs. 10b and 10d) are consistently 180° apart for all x/c values in the far region, suggesting that wake acceleration is likely more airfoil-shape dependent than motion dependent. Further study on a wide range of airfoil shapes and motions would be needed to fully understand the underlying dynamics of this wake acceleration.

Although it is interesting to understand the phase relationship between the hydrofoils, the power consumption is a more critical aspect of the interaction. The data shown in Fig. 3 demonstrate that the power consumption of the follower had a sinusoidal relationship with phase offset, but it also varied as a function of x/c and z/b. Equation (14) was developed around this sinusoidal relationship and uses Eqs. (15) and (16), which were empirically defined using the data from the current study:

$$C_P = \Delta C_P \cos(\phi - \phi_{\overline{C_P}, \min} + 180 \text{ deg}) + C_{P, \text{offset}}$$
 (14)

$$2\Delta C_P = C_1(x/c)^{C_2} + C_3 + \begin{cases} 0 & z/b \le 0.15x/c \\ C_4(z/b) & z/b > 0.15x/c \end{cases}$$
(15)

$$C_{P,\text{offset}} = C_5(x/c)^3 + C_6(x/c)^2 + C_7(x/c) + C_8$$
 (16)

where ΔC_P is an amplitude modifier that is dependent on the streamwise and spanwise positions, $\phi_{\overline{C_P}, \min}$ is the phase offset of minimum power consumption [Eq. (13)], and $C_{P, \text{offset}}$ is an offset term that is dependent on the streamwise location. Equation (15) uses a best-fit exponential function for streamwise spacing. C_{1-4} are best-fit coefficients based on the experimental results. A piecewise function was required to account for the vortex wake contraction and its interaction with the follower. As shown in Fig. 8, the power remained constant for small spanwise spacings, before linearly decaying. $C_{P, \text{offset}}$ was defined using a third-order best-fit curve of the experimental data.

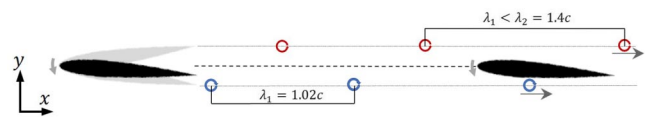


Fig. 11 Acceleration of wake.

Table 3 Empirical coefficients for follower power consumption

Parameter	Value
$\overline{C_1}$	0.002546
C_2	-18.34
C_3	0.1281
C_4	-0.115
C_5	-0.3929
C_6	0.9769
C_7	-0.8057
C_8	0.6633

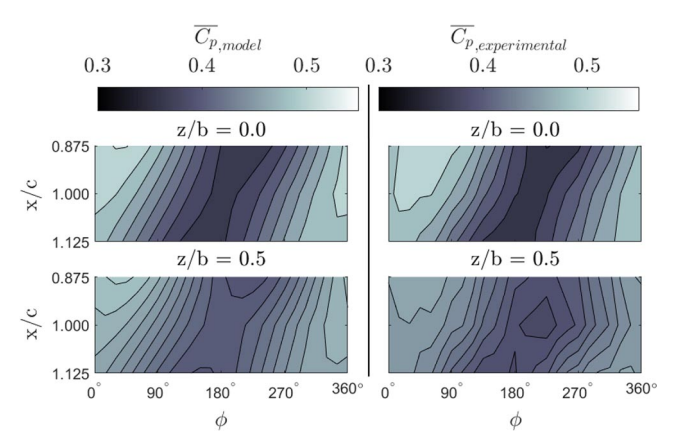


Fig. 12 Comparison of predicted and experimental average power consumption for the follower hydrofoil.

The empirically derived coefficients C_{1-8} are shown in Table 3 for reference. It is likely that these coefficients are dependent on the airfoil shape, aspect ratio, and other factors. However, it is expected that the general outline of Eqs. (14–16) applied to all tandem hydrofoil cases in the far region. A comparison of the experimental data and data modeling using Eqs. (14–16) and the coefficients in Table 3 is shown in Fig. 12. The model was applied only to the far region but exhibited close alignment with the experimental data.

IV. Conclusions

An experimental investigation of tandem oscillating hydrofoils was done to evaluate the effects of spanwise spacing. A variety of relative streamwise spacings, spanwise spacings, and phase offsets were tested at a constant Strouhal number; and the hydrodynamic forces acting on both hydrofoils were recorded. The time-averaged thrust production and power consumption of the follower were strongly affected by the presence of the leader. The magnitude of the changes in the follower's hydrodynamic performance from that of an isolated foil decreased with increasing streamwise spacing, and two distinct streamwise spacing regions were identified: a near and a far. A delineation between these near and far regions was found at around x/c = 0.875. In the far region, the leader was largely unaffected by the presence of the follower; and the follower's performance trended toward its isolated value with increasing streamwise spacing. The transition to the near region was marked by a decrease in maximum average power consumption by both hydrofoils and an increase in the propulsive efficiency of the follower hydrofoil. The introduction of spanwise spacing had limited effects on the performance characteristics of the leader, regardless of streamwise spacing or phase offset relative to the follower. In all configurations tested, the spanwise forces acting on the hydrofoils were small, indicating that there were no net forces driving the hydrofoils toward any particular spanwise configuration.

Distinct trends with spanwise spacing were observed for the follower, which were linked to the spanwise contraction of the vortical wake structure shed by the leader. Below a critical spanwise spacing, which was dependent on the rate of wake contraction and streamwise spacing, there was little to no change in performance. This corresponded to a region where there was no change in the portion of the follower hydrofoil's span interacting with the incoming wake. Spanwise spacings beyond a critical value resulted in a monotonic decrease in the hydrodynamic performance of the follower, trending toward the isolated performance of the follower.

Finally, a simple model was developed for the average power consumption of the follower hydrofoil as a function of streamwise spacing, spanwise spacing, and phase offset relative to the leader, specifically for the far streamwise region. This model was derived empirically from the experimental data gathered and produced results that closely matched experimental results. This demonstrates the feasibility of using simple models, such as the one developed here to predict the performance of hydrofoils, for a variety of configurations that may help provide further insight into the underlying flow physics.

Appendix: Experimental Uncertainty Analysis

Uncertainty was calculated using the methods outlined by Figliola and Beasley [48] and, in a similar manner, employed by Stutz et al. [52], which takes into account random uncertainty S and bias uncertainty b'. Random uncertainty quantifies the variability in each input, and bias uncertainty quantifies measurement accuracy and error. The equations used for the power calculations are given in Eqs. (A1–A7). Random and bias uncertainty values are given in Table A1. The resulting uncertainties in the power coefficient, thrust coefficient, lift coefficient, and efficiency are shown in Table A2:

$$P(t) = T_Z \dot{\theta} \tag{A1}$$

$$S_P = \sqrt{\left[\frac{\partial P}{\partial T_Z} S_{T_Z}\right]^2 + \left[\frac{\partial P}{\partial \dot{\theta}} S_{\dot{\theta}}\right]^2}$$
 (A2)

$$b_P' = \sqrt{\left[\frac{\partial P}{\partial T_Z}b_{T_Z}'\right]^2 + \left[\frac{\partial P}{\partial \dot{\theta}}b_{\dot{\theta}}'\right]^2}$$
 (A3)

$$C_P = P/0.5\rho bc U_{\infty}^3 \tag{A4}$$

Table A2 Random and bias uncertainties for isolated hydrofoils

Variable	S_x	b_x'
C_T , leader	±0.010	±0.013
C_T , follower	± 0.003	± 0.013
C_P , leader	± 0.0002	± 0.040
C_P , follower	± 0.0001	± 0.040
η , leader	±3%	$\pm 1\%$
η , follower	±1%	±1%

$$u_{C_P} = \pm \sqrt{S_{C_P}^2 + b_{C_P}'^2}$$
 (A7)

Acknowledgments

This work was supported by the National Science Foundation (NSF) under Program Director Ronald Joslin in Fluid Dynamics within Chemical, Biological, Environmental, and Transport Systems (CBET) on NSF CAREER award number 1653181, as well as by the Office of Naval Research under Program Director Robert Brizzolara on Multi-disciplinary University Research Initiative (MURI) grant number N00014-22-1-2616. Research was further sponsored by Combat Capabilities Development Command (DEVCOM) of the U.S. Army Research Laboratory and was accomplished under cooperative agreement number W911NF-19-2-0197. The views and conclusions contained in this document are those of the authors and should not be interpreted as representing the official policies, either expressed or implied, of DEVCOM of the U.S. Army Research Laboratory or the U.S. Government.

References

- [1] Kentfield, J. A. C., "Formation Flight and Much More," AIAA Journal, Vol. 45, No. 8, 2007, pp. 1795–1797. https://doi.org/10.2514/1.31222
- [2] Weimerskirch, H., Martin, J., Clerquin, Y., Alexandre, P., and Jiraskova, S., "Energy Saving in Flight Formation—Pelicans Flying in a 'V' Can Glide for Extended Periods Using the Other Birds' Air Streams."

$$S_{C_P} = \sqrt{\left[\frac{\partial C_P}{\partial P} S_P\right]^2 + \left[\frac{\partial C_P}{\partial \rho} S_\rho\right]^2 + \left[\frac{\partial C_P}{\partial b} S_b\right]^2 + \left[\frac{\partial C_P}{\partial c} S_c\right]^2 + \left[\frac{\partial C_P}{\partial U_\infty} S_{U_\infty}\right]^2}$$
(A5)

$$b_{C_P}' = \sqrt{\left[\frac{\partial C_P}{\partial P}b_P'\right]^2 + \left[\frac{\partial C_P}{\partial \rho}b_\rho'\right]^2 + \left[\frac{\partial C_P}{\partial b}b_b'\right]^2 + \left[\frac{\partial C_P}{\partial c}b_c'\right]^2 + \left[\frac{\partial C_P}{\partial U_\infty}b_{U_\infty}'\right]^2}$$
(A6)

Table A1 Uncertainty calculation inputs

Variable	S_x	b_x'
b, m	0	±4E-4
c, m	0	±4E-4
F_x , N	$\pm \sigma_{F_x}/\sqrt{N_{F_x}}$	$\pm 1.125\% F_x$
F_y , N	$\pm \sigma_{F_{_{\mathrm{y}}}}/\sqrt{N_{F_{_{\mathrm{y}}}}}$	$\pm 1.125\% F_{y}$
F_z , N	$\pm \sigma_{F_z}/\sqrt{N_{F_z}}$	$\pm 1.125\% F_z$
T_z , N·mm	$\pm \sigma_{T_z}/\sqrt{N_{T_z}}$	$\pm 1.125\% T_z$
U_{∞} , m/s	$\pm 1\% U_{\infty}$	$\pm 1\% U_{\infty}$
θ , deg	$\pm \sigma_{ heta}/\sqrt{N_{ heta}}$	± 0.025
$\dot{\theta}$, deg/s	$\pm \sigma_{\dot{ heta}}/\sqrt{N_{\dot{ heta}}}$	$\pm 5\%\dot{ heta}$
ρ , kg/m ³	0	± 0.5

- *Nature*, Vol. 413, No. 6857, 2001, pp. 697–698. https://doi.org/10.1038/35099670
- [3] Portugal, S. J., Hubel, T. Y., Fritz, J., Heese, S., Trobe, D., Voelkl, B., Hailes, S., Wilson, A. M., and Usherwood, J. R., "Upwash Exploitation and Downwash Avoidance by Flap Phasing in IBIS Formation Flight," *Nature*, Vol. 505, No. 7483, 2014, pp. 399–402. https://doi.org/10.1038/nature12939
- [4] Sfakiotakis, M., Lane, D., and Davies, J., "Review of Fish Swimming Modes for Aquatic Locomotion," *IEEE Journal of Oceanic Engineering*, Vol. 24, No. 2, 1999, pp. 237–252. https://doi.org/10.1109/48.757275
- [5] Triantafyllou, G., Triantafyllou, M., and Grosenbaugh, M., "Optimal Thrust Development in Oscillating Foils with Application to Fish Propulsion," *Journal of Fluids and Structures*, Vol. 7, No. 2, 1993, pp. 205–224. https://doi.org/10.1006/jfls.1993.1012
- [6] Taylor, G., Nudds, R., and Thomas, A., "Flying and Swimming Animals Cruise at a Strouhal Number Tuned for High Power Efficiency," *Nature*,

- Vol. 425, No. 6959, 2003, pp. 707–711. https://doi.org/10.1038/nature02000
- [7] Lighthill, M., "Hydromechanics of Aquatic Animal Propulsion," *Annual Review of Fluid Mechanics*, Vol. 1, No. 1, 1969, pp. 413–446. https://doi.org/10.1146/annurev.fl.01.010169.002213
- [8] Blickhan, R., Krick, C., Zehren, D., Nachtigall, W., and Breithaupt, T., "Generation of a Vortex Chain in the Wake of a Subundulatory Swimmer," *Natuwissenchaften*, Vol. 79, No. 5, 1992, pp. 220–221. https://doi.org/10.1007/BF01227131
- [9] Triantafyllou, G., Triantafyllou, M., and Grosenbaugh, M., "Optimal Thrust Development in Oscillating Foils with Application to Fish Propulsion," *Journal of Fluids and Structures*, Vol. 7, No. 2, 1993, pp. 205–224. https://doi.org/10.1006/jfls.1993.1012
- [10] Müller, U. K., Van Den Heuvel, B. L. E., Stamhuis, E. J., and Videler, J. J., "Fish Foot Prints: Morphology and Energetics of the Wake Behind a Continuously Swimming Mullet (*Chelon labrosus risso*)," *Journal of Experimental Biology*, Vol. 200, No. 22, 1997, pp. 2893–2906.
- [11] Vandenberghe, N., Zhang, J., and Childress, S., "Symmetry Breaking Leads to Forward Flapping Flight," *Journal of Fluid Mechanics*, Vol. 506, May 2004, pp. 147–155. https://doi.org/10.1017/S0022112004008468
- [12] Buchholz, J. H. J., and Smits, A. J., "The Wake Structure and Thrust Performance of a Rigid Low-Aspect-Ratio Pitching Panel," *Journal of Fluid Mechanics*, Vol. 603, May 2008, pp. 331–365. https://doi.org/10.1017/S0022112008000906
- [13] Andersen, A., Bohr, T., Schnipper, T., and Walther, J. H., "Wake Structure and Thrust Generation of a Flapping Foil in Two-Dimensional Flow," *Journal of Fluid Mechanics*, Vol. 812, Feb. 2017, Paper R4. https://doi.org/10.1017/jfm.2016.808
- [14] Smits, A. J., "Undulatory and Oscillatory Swimming," *Journal of Fluid Mechanics*, Vol. 874, Sept. 2019, Paper P1. https://doi.org/10.1017/jfm.2019.284
- [15] Liao, J. C., "A Review of Fish Swimming Mechanics and Behaviour in Altered Flows," *Philosophical Transactions of the Royal Society of Biological Sciences*, Vol. 362, No. 1487, 2007, pp. 1973–1993. https://doi.org/10.1098/rstb.2007.2082
- [16] Lauder, G. V., "Fish Locomotion: Recent Advances and New Directions," *Annual Review of Marine Science*, Vol. 7, Jan. 2015, pp. 521–545. https://doi.org/10.1146/annurev-marine-010814-015614
- [17] Zhang, D., Zhang, J.-D., and Huang, W.-X., "Physical Models and Vortex Dynamics of Swimming and Flying: A Review," *Acta Mechanica*, Vol. 233, No. 4, 2022, pp. 1249–1288. https://doi.org/10.1007/s00707-022-03192-9
- [18] Beal, D., Hover, F., Triantafyllou, M., Liao, J., and Lauder, G., "Passive Propulsion in Vortex Wakes," *Journal of Fluid Mechanics*, Vol. 549, Feb. 2006, pp. 385–402. https://doi.org/10.1017/S0022112005007925
- [19] Partridge, B. L., Pitcher, T., Cullen, J. M., and Wilson, J., "The 3-Dimensional Structure of Fish Schools," *Behavioral Ecology of Sociobiology*, Vol. 6, No. 4, 1980, pp. 277–288. https://doi.org/10.1007/BF00292770
- [20] Partridge, B., and Pitcher, T., "Evidence Against a Hydrodynamic Function for Fish Schools," *Nature*, Vol. 279, No. 5712, 1979, pp. 418–419. https://doi.org/10.1038/279418a0
- [21] Weihs, D., "Hydrodynamics of Fish Schooling," *Nature*, Vol. 241, No. 5387, 1973, pp. 290–291. https://doi.org/10.1038/241290a0
- [22] Cushing, D., and Harden Jones, F., "Why Do Fish School," *Nature*, Vol. 218, No. 5145, 1968, pp. 918–920. https://doi.org/10.1038/218918b0
- [23] Breder, C., "On Survival Value of Fish Schools," Zoologica-New York, Vol. 52, No. 2, 1967, pp. 25–40.
- [24] Herskin, J., and Steffensen, J., "Energy Savings in Sea Bass Swimming in a School: Measurements of Tail Beat Frequency and Oxygen Consumption at Different Swimming Speeds," *Journal of Fish Biology*, Vol. 53, No. 2, 1998, pp. 366–376. https://doi.org/10.1111/j.1095-8649.1998.tb00986.x
- [25] Killen, S. S., Marras, S., Steffensen, J. F., and McKenzie, D. J., "Aerobic Capacity Influences the Spatial Position of Individuals Within Fish Schools," *Proceeding of the Royal Society of London, Series B: Bio-logical Sciences*, Vol. 279, No. 1727, 2012, pp. 357–364. https://doi.org/10.1098/rspb.2011.1006
- [26] Partridge, B., and Pitcher, T., "The Sensory Basis of Fish Schools— Relative Roles of Lateral Line and Vision," *Journal of Comparative Physiology*, Vol. 135, No. 4, 1980, pp. 315–325. https://doi.org/10.1007/BF00657647

- [27] Ashraf, I., Godoy-Diana, R., Halloy, J., Collignon, B., and Thiria, B., "Synchronization and Collective Swimming Patterns in Fish (Hemigrammus bleheri)," Journal of the Royal Society Interface, Vol. 13, No. 123, 2016, Paper 20160734. https://doi.org/10.1098/rsif.2016.0734
- [28] Mekdara, P. J., Nasimi, F., Schwalbe, M. A. B., and Tytell, E. D., "Tail Beat Synchronization During Schooling Requires a Functional Posterior Lateral Line System in Giant Danios, *Devario Aequipinnatus*," *Integra*tive and Comparative Biology, Vol. 61, No. 2, 2021, pp. 427–441. https://doi.org/10.1093/icb/icab071
- [29] Mekdara, P. J., Schwalbe, M. A., Coughlin, L. L., and Tytell, E. D., "The Effects of Lateral Line Ablation and Regeneration in Schooling Giant Danios," *Journal of Experimental Biology*, Vol. 221, No. 8, 2018, Paper jeb175166.
- [30] Liao, J., Beal, D., Lauder, G., and Triantafyllou, M., "The Karman Gait: Novel Body Kinematics of Rainbow Trout Swimming in a Vortex Street," *Journal of Experimental Biology*, Vol. 206, No. 6, 2003, pp. 1059–1073. https://doi.org/10.1242/jeb.00209
- [31] Harvey, S. T., Muhawenimana, V., Muller, S., Wilson, C. A. M. E., and Denissenko, P., "An Inertial Mechanism Behind Dynamic Station Holding by Fish Swinging in a Vortex Street," *Scientific Reports*, Vol. 12, No. 1, 2022, Paper 12660. https://doi.org/10.1038/s41598-022-16181-8
- [32] Thandiackal, R., and Lauder, G., "In-Line Swimming Dynamics Revealed by Fish Interacting with a Robotic Mechanism," *Elife*, Vol. 12, Feb. 2023, Paper e81392.
- [33] Colgan, D., Xu, B., Wei, M., and Hrynuk, J., "3D Vortical Structure of Multiple Moving Spheroids Under Adjoint-Based Optimal Control," AIAA SciTech 2023 Forum, AIAA Paper 2023-0458, 2023.
- [34] Xu, B., Colgan, D., Wei, M., and Hrynuk, J. T., "Adjoint-Based Optimal Control on Flows with Multiple Moving Cylinders in Tandem," AIAA SciTech 2023 Forum, AIAA Paper 2023-0457, 2023.
- [35] Boschitsch, B. M., Dewey, P. A., and Smits, A. J., "Propulsive Performance of Unsteady Tandem Hydrofoils in an In-Line Configuration," *Physics of Fluids*, Vol. 26, No. 5, 2014, Paper 051901. https://doi.org/10.1063/1.4872308
- [36] Kurt, M., and Moored, K. W., "Flow Interactions of Two- and Three-Dimensional Networked Bio-Inspired Control Elements in an In-Line Arrangement," *Bioinspiration and Biomimetics*, Vol. 13, No. 4, 2018, Paper 045002. https://doi.org/10.1088/1748-3190/aabf4c
- [37] King, J. T., Kumar, R., and Green, M. A., "Experimental Observations of the Three-Dimensional Wake Structures and Dynamics Generated by a Rigid, Bioinspired Pitching Panel," *Physical Review Letters*, Vol. 3, No. 3, 2018, Paper 034701. https://doi.org/10.1103/PhysRevFluids.3.034701
- [38] Mivehchi, A., Zhong, Q., Kurt, M., Quinn, D. B., and Moored, K. W., "Scaling Laws for the Propulsive Performance of a Purely Pitching Foil in Ground Effect," *Journal of Fluid Mechanics*, Vol. 919, July 2021, Paper R1. https://doi.org/10.1017/jfm.2021.361
- [39] Newbolt, J. W., Zhang, J., and Ristroph, L., "Lateral Flow Interactions Enhance Speed and Stabilize Formations of Flapping Swimmers," *Physical Review Fluids*, Vol. 7, No. 6, 2022, Paper L061101. https://doi.org/10.1103/PhysRevFluids.7.L061101
- [40] Arranz, G., Flores, O., and Garcia-Villalba, M., "Flow Interaction of Three-Dimensional Self-Propelled Flexible Plates in Tandem," *Journal* of Fluid Mechanics, Vol. 931, Jan. 2021, Paper A5. https://doi.org/10.1017/jfm.2021.918
- [41] Heydari, S., and Kanso, E., "School Cohesion, Speed and Efficiency are Modulated by the Swimmers Flapping Motion," *Journal of Fluid Mechanics*, Vol. 922, Sept. 2021, Paper A27. https://doi.org/10.1017/jfm.2021.551
- [42] Ryu, J., Yang, J., Park, S. G., and Sung, H. J., "Phase-Mediated Locomotion of Two Self-Propelled Flexible Plates in a Tandem Arrangement," *Physics of Fluids*, Vol. 32, No. 4, 2020, Paper 041901. https://doi.org/10.1063/5.0005489
- [43] Newbolt, J. W., Zhang, J., and Ristroph, L., "Flow Interactions Between Uncoordinated Flapping Swimmers Give Rise to Group Cohesion," Proceedings of the National Academy of Sciences of the United States of America, Vol. 116, No. 7, 2019, pp. 2419–2424. https://doi.org/10.1073/pnas.1816098116
- [44] Becker, A. D., Masoud, H., Newbolt, J. W., Shelley, M., and Ristroph, L., "Hydrodynamic Schooling of Flapping Swimmers," *Nature Communications*, Vol. 6, No. 1, 2015, Paper 8514. https://doi.org/10.1038/ncomms9514
- [45] Li, L., Nagy, M., Graving, J. M., Bak-Coleman, J., Xie, G., and Couzin, I. D., "Vortex Phase Matching as a Strategy for Schooling in Robots and

- in Fish," *Nature Communications*, Vol. 11, No. 1, 2020, Paper 5408. https://doi.org/10.1038/s41467-020-19086-0
- [46] Fishman, G., Wolfinger, M., and Rockwell, D., "The Structure of a Trailing Vortex from a Perturbed Wing," *Journal of Fluid Mechanics*, Vol. 824, Aug. 2017, pp. 701–721. https://doi.org/10.1017/jfm.2017.331
- [47] Elger, D. F., Williams, B. C., Crowe, C. T., and Roberson, J. A., Engineering Fluid Mechanics, 10th ed., Wiley, Hoboken, NJ, 2012.
- [48] Figliola, R. S., and Beasley, D. E., Theory and Design for Mechanical Measurements, Wiley, Hoboken, NJ, 2020, pp. 154–160.
- [49] Senturk, U., and Smits, A. J., "Reynolds Number Scaling of the Propulsive Performance of a Pitching Airfoil," *AIAA Journal*, Vol. 57, No. 7, 2019, pp. 2663–2669. https://doi.org/10.2514/1.1058371
- [50] Poudel, N., Yu, M., and Hrynuk, J. T., "Impacts of Unsteady Flow Environments on the Propulsive Performance of Oscillating Foils," *AIAA Journal*, Vol. 61, No. 3, 2023, pp. 1210–1223.
- [51] Epps, B. P., Muscutt, L. E., Roesler, B. T., Weymouth, G. D., and Ganapathisubramani, B., "On the Interfoil Spacing and Phase Lag of Tandem Flapping Foil Propulsors," *Journal of Ship Production and Design*, Vol. 33, No. 4, 2017, pp. 276–282.
- [52] Stutz, C., Hrynuk, J., and Bohl, D., "Investigation of Static Wings Interacting with Vertical Gusts of Indefinite Length at Low Reynolds Numbers," *Experiments in Fluids*, Vol. 63, No. 5, 2022, Paper 82.

P. Lavoie Associate Editor